JCI insight

RESEARCH ARTICLE

Endothelial mitochondria determine rapid barrier failure in chemical lung injury

Rebecca F. Hough,[1,2] Mohammad N. Islam,[1] Galina A. Gusarova,[1] Guangchun Jin,[1] Shonit Das,[1] and Jahar Bhattacharya[1]

[1]Lung Biology Lab, Department of Medicine, and [2]Department of Pediatrics, Columbia University Vagelos College of Physicians and Surgeons, New York, New York, USA.

Acid aspiration, which can result from several etiologies, including postoperative complications, leads to direct contact of concentrated hydrochloric acid (HCl) with the alveolar epithelium. As a result, rapid endothelial activation induces alveolar inflammation, leading to life-threatening pulmonary edema. Because mechanisms underlying the rapid endothelial activation are not understood, here we determined responses in real time through optical imaging of alveoli of live mouse lungs. By alveolar micropuncture, we microinfused concentrated HCl in the alveolar lumen. As expected, acid contact with the epithelium caused rapid, but transient, apical injury. However, there was no concomitant membrane injury to the endothelium. Nevertheless, H_2O_2-mediated epithelial-endothelial paracrine signaling induced endothelial barrier failure, as detected by microvascular dextran leakage and lung water quantification. Remarkably, endothelial mitochondria regulated the barrier failure by activating uncoupling protein 2 (UCP2), thereby inducing transient mitochondrial depolarization that led to cofilin-induced actin depolymerization. Knockdown, or endothelium-targeted deletion of UCP2 expression, blocked these responses, including pulmonary edema. To our knowledge, these findings are the first to mechanistically implicate endothelial mitochondria in acid-induced barrier deterioration and pulmonary edema. We suggest endothelial UCP2 may be a therapeutic target for acid-induced acute lung injury.

Introduction

Chemical injury to the alveolar epithelium of the lung induces inflammatory responses that can cause tissue edema and organ dysfunction. Thus, in acid-induced acute lung injury (ALI), although direct contact with aspirated acid causes primary injury to the alveolar epithelium (1), pulmonary edema results from rapidly induced endothelial barrier failure in adjoining microvessels (2, 3). Proinflammatory epithelial-endothelial crosstalk signaling occurs in minutes (4). However, it is not clear whether this rapid crosstalk also induces rapid barrier failure. Therapy for ALI might be better served through better understanding of these mechanisms.

An unresolved question relates to the extent to which inhaled injurious agents arriving in the alveoli cause epithelial versus endothelial injury. The close proximity of the endothelial and epithelial membranes, which are separated by 1–2 μm in the alveolar wall (5), predicate that both membranes might be injured. On the other hand, the highly efficient epithelial barrier might protect the endothelium from direct injury. Nevertheless, contact of the epithelium with the injurious agent could transmit a proinflammatory signal to the uninjured endothelium.

Here, we addressed these issues in the context of acid-induced alveolar injury through in situ optical imaging of live alveoli. In conjunction with the alveolar micropuncture technique, the optical approach enables cell-specific localization of injury, as quantified by the loss of aqueous dye from the cytosol (1). Applying this approach, we noted that alveolar microinfusion of concentrated hydrochloric acid (HCl) caused epithelial but not endothelial injury. However, surprisingly, endothelial mitochondria underwent rapid depolarization. Because injury-induced mitochondrial responses are unreported (to our knowledge) in lung endothelia, we followed up on our findings to determine the possible role of the mitochondrial depolarization in acid-induced barrier dysregulation.

Mitochondria play multiple roles in cell function, including calcium mobilization, H_2O_2 generation, and release of metabolites, all of which could affect endothelial barrier integrity. Mitochondria pump H^+ ions to establish a proton gradient across the inner mitochondrial membrane (IMM), resulting in a negative matrix

Authorship note: SD is deceased.

Conflict of interest: The authors have declared that no conflict of interest exists.

Submitted: August 21, 2018
Accepted: December 20, 2018
Published: February 7, 2019

Reference information:
JCI Insight. 2019;4(3):e124329.
https://doi.org/10.1172/jci.insight.124329.

potential. Induction of the oxidant-activated channel, uncoupling protein 2 (UCP2), activates a proton channel in the IMM that could dissipate the proton gradient, causing mitochondrial depolarization (6–8). We report below our findings that alveolar injury–induced depolarization of endothelial mitochondria caused cofilin-dependent actin depolymerization and endothelial barrier failure. To our knowledge, these findings are the first to directly link mitochondrial dysfunction with lung microvascular hyperpermeability.

Results

Alveolar acid instillation causes epithelium-specific membrane injury. To determine the site of membrane injury caused by alveolar microinstillation of concentrated HCl (pH 1.1), we viewed alveoli of isolated, blood-perfused mouse lungs (IPLs) by live confocal microscopy (9, 10). We separately loaded the alveolar epithelium and the adjoining endothelium with cytosol-targeting calcein acetoxymethyl (AM) dyes expressing different pseudocolors. Although the alveolar epithelium and endothelium are closely juxtaposed in the alveolar wall, discreet pseudocolor markings enabled differential detection of these cell types (Figure 1A). Alveolar microinjection of HCl decreased alveolar epithelial fluorescence (Figure 1, B and C), affirming that HCl contact with the alveolar wall rapidly induces membrane leaks in the epithelium. By contrast, endothelial fluorescence remained unchanged (Figure 1, B and C), indicating that the alveolar HCl injection did not damage the endothelial membrane. Alveolar injection of buffer had no effect. Successful calcein reloading of alveolar epithelium 30 minutes after the HCl injection (Figure 1, B and C) affirmed that the membrane damage was transient (1). We conclude that alveolar HCl microinjection caused epithelial, but not endothelial, membrane injury.

Alveolar acid induces transient depolarization of endothelial mitochondria. H_2O_2 release following alveolar HCl microinjection (1) may cause endothelial mitochondrial dysfunction. To evaluate this possibility, we detected endothelial mitochondria by the fluorescence of the mitochondria-targeted, potentiometric dye, TMRE (Figure 1B). Vascular microinjection of the detergent Triton X-100 decreased endothelial fluorescence of calcein, but not TMRE (Supplemental Figure 1; supplemental material available online with this article; https://doi.org/10.1172/jci.insight.124329DS1), affirming that TMRE localized to endothelial mitochondria. Although TMRE fluorescence was steady at baseline, alveolar HCl microinjection decreased the fluorescence in 10 minutes (Figure 1, B and C), indicating that the acid injection depolarized the mitochondria. However, 30 minutes later we successfully reloaded TMRE in endothelial mitochondria (Figure 1, B and C). Hence, subsequent to depolarization, the mitochondria repolarized within a short period, ruling out the presence of apoptosis (11). Thus, alveolar HCl microinjection caused rapid, but transient, depolarization of endothelial mitochondria.

To determine whether the mitochondrial depolarization resulted from alveolar HCl–initiated H_2O_2 diffusion from the alveolar epithelium, we transfected the alveolar epithelium with catalase. HCl injection in catalase-transfected alveoli failed to induce endothelial TMRE loss (Figure 1D), indicating that catalase-induced inhibition of H_2O_2 release inhibited the depolarization. Transfection of empty vector had no inhibitory effect. In IPLs with catalase-transfected alveolar epithelium, direct microvascular injection of H_2O_2 caused endothelial TMRE loss (Supplemental Figure 2), ruling out nonspecific factors in the catalase-induced inhibitory effect. Pretreatment with the antioxidant *N*-acetyl cysteine, given by the vascular route, also prevented alveolar HCl–induced TMRE loss in the endothelium (Figure 1D), indicating that the mitochondrial depolarization can be inhibited pharmacologically. Vascular pretreatment with the cell-permeant calcium chelator BAPTA (1,2-bis[*o*-aminophenoxy]ethane-*N*,*N*,*N*′,*N*′-tetraacetic acid) did not prevent alveolar HCl–induced endothelial TMRE loss (Supplemental Figure 3), ruling out a role for the cytosolic calcium in the mitochondrial depolarization. Previously, our group showed that macrophage depletion by instillation of clodronate did not prevent alveolar HCl–induced microvascular ROS increase, suggesting that the epithelial-endothelial transfer of ROS is not macrophage dependent (1). Thus, we conclude that alveolar HCl–induced mitochondrial depolarization in the endothelium resulted from rapid paracrine transfer of H_2O_2 from the alveolar epithelium.

Alveolar acid induces UCP2-dependent endothelial mitochondrial depolarization. We considered that paracrine H_2O_2 could activate the endothelial mitochondrial protein UCP2, a protein activated by ROS (6, 7). To evaluate UCP2 distribution in lung capillaries, we infused fluorescently labeled UCP2 antibody into venular capillaries. The resulting vascular fluorescence indicated extensive UCP2 expression in the capillary network (Figure 2A).

To determine whether UCP2 activation caused alveolar HCl–induced endothelial mitochondrial depolarization, we delivered UCP2-targeted siRNA (siUCP2) by the microvascular route to load the endothelium. As compared with scrambled siRNA (scRNA), which had no effect, 2 days after siUCP2 treatment UCP2 protein decreased by 40%, as detected by immunoblots using different antibodies against separate

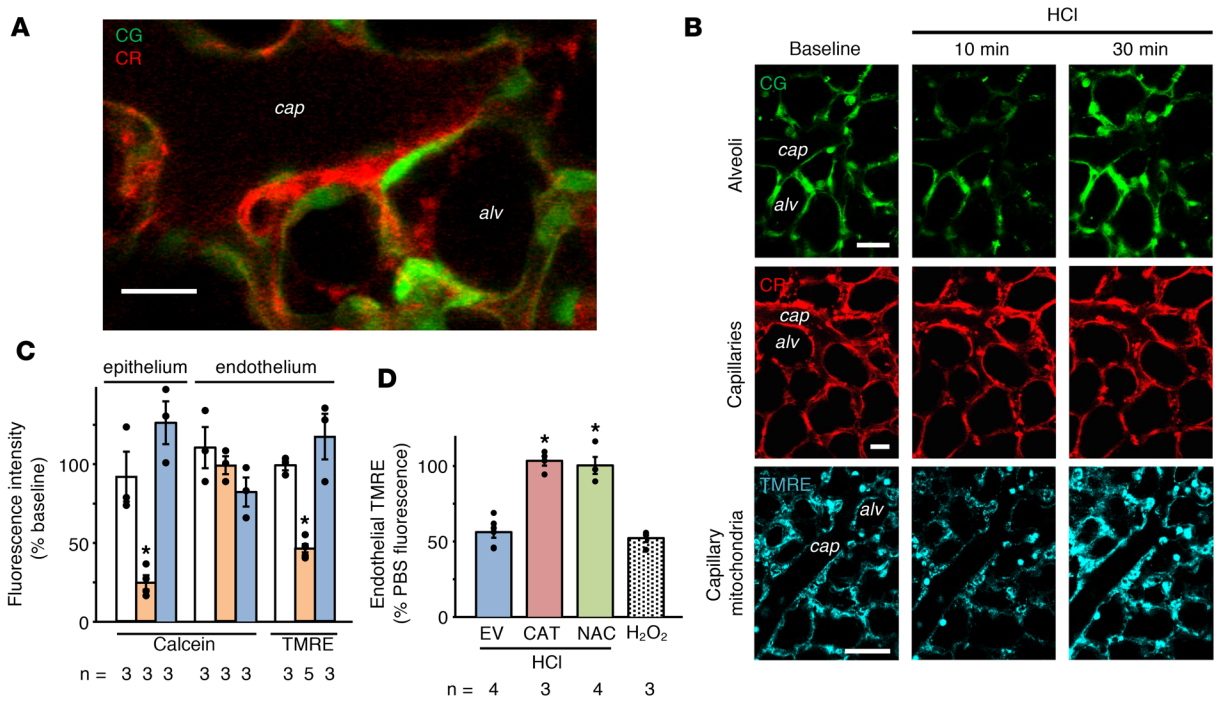

Figure 1. Fluorescence responses to intra-alveolar HCl injection in the alveolar epithelium and endothelium. Epithelial and endothelial cytosols were loaded with calcein green (CG, 10 μM) and calcein red (CR, 2.5 μM), respectively. (**A**) High-power confocal image shows separation of the alveolar epithelium from the juxtaposed capillary endothelium. *Cap*, capillary lumen; *alv*, alveolus. *n* = 5 lungs. Scale bar: 20 μm. (**B**) Fluorescence of CG, CR, and tetramethylrhodamine ethyl ester (TMRE, intravascularly, 2 μM) at indicated time points before (baseline) and after alveolar HCl injection. Images at 30 minutes were obtained after repeat injections of CG and TMRE. Scale bars: 20 μm. (**C**) Bars are quantifications in cytosol (calcein) and mitochondria (TMRE) for the indicated cell types following alveolar injections of PBS or HCl. White, PBS; orange, 10 minutes after HCl; blue, 30 minutes after HCl. **P* < 0.05 versus PBS. (**D**) Effects of indicated treatments on endothelial TMRE following alveolar HCl or microvascular H_2O_2 injection. EV, intranasal empty vector; CAT, alveolar catalase transfection; NAC, intravascular *N*-acetyl cysteine. **P* < 0.05 versus EV. Data are shown as mean ± SEM for the number of injections indicated by dots. *n*, number of lungs. One-way ANOVA with post hoc Bonferroni's test was used to determine statistical differences between groups.

UCP2 epitopes (Figure 2B). These findings affirmed that vascular delivery of siUCP2 caused marked knockdown of UCP2 in the endothelium. In mice with UCP2 knockdown (UCP2-KD), alveolar HCl injection failed to cause loss of endothelial TMRE fluorescence (Figure 2C), although the loss occurred in mice that received scRNA. Further, direct microvascular H_2O_2 infusion in UCP2-KD mice failed to decrease TMRE fluorescence, while the decrease occurred in mice given scRNA (Figure 2C). We considered that delivery of siUCP2 by the microvascular route might cause leakage of the siRNA into the alveolar epithelium and subsequent UCP2 knockdown there. Hence, in siUCP2-treated lungs, we loaded TMRE in the alveolar epithelium. Alveolar HCl injection decreased the alveolar epithelial TMRE fluorescence, indicating that mitochondrial depolarization occurred in the alveolar epithelium (Supplemental Figure 4), hence ruling out the possibility that siUCP2 leaked across the microvascular barrier, causing UCP2 knockdown in the alveolar epithelium. Taking these findings together, we conclude that in the endothelium, alveolar HCl–induced H_2O_2 activated UCP2, depolarizing mitochondria.

To determine the effects of endothelium-specific UCP2 deletion, we bred UCP2-floxed mice with Tie2-Cre mice to obtain *UCP2$^{fl/fl}$:Tie2-Cre*. Our lab has previously used Tie2 mice to achieve endothelium-specific KO (12, 13). Although the Tie2 promoter is also expressed in cells of the myeloid lineage (14), no myeloid cells were present in the imaging field. Alveolar HCl injection failed to cause endothelial TMRE loss in mice expressing *UCP2$^{fl/fl}$:Tie2-Cre*, although the loss was evident in littermate controls expressing only the floxed allele (Figure 2C). These findings support our interpretation that activation of endothelial UCP2 underlies alveolar HCl–induced endothelial mitochondrial depolarization.

Alveolar acid induces UCP2-dependent barrier loss. To determine the endothelial barrier effects of alveolar HCl injection, we gave a microvascular injection of fluorescein-labeled 70-kDa dextran (FITC-D70). At baseline, or after alveolar PBS injection, microvessels efficiently retained FITC-D70 with no transvascular

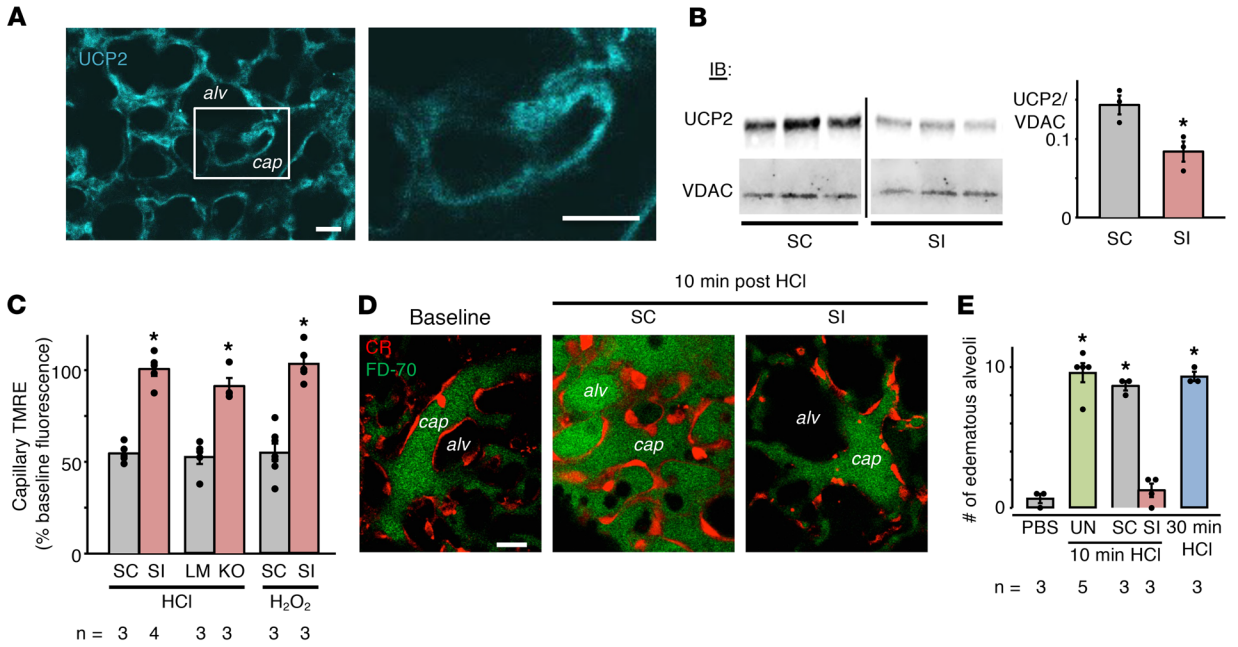

Figure 2. Effects of alveolar HCl–induced endothelial UCP2 activation. (**A**) Confocal image shows endothelial immunofluorescence in lung capillaries (*cap*) at low magnification. The other image shows the region of interest marked by the rectangle at high magnification. Capillaries were microinfused with 4% paraformaldehyde and 0.2% Triton X-100 (45 minutes), followed by Alexa Fluor 633–labeled anti–UCP2 goat polyclonal antibody (120 ng/ml, 30 minutes). Capillaries were buffer washed (5 minutes). n = 4 lungs. Scale bar: 20 μm. (**B**–**E**) Data are for analyses carried out 48 hours after tail vein injection of indicated siRNA. (**B**) Gel and bars show immunoblotting (IB) and densitometry of mitochondria isolated from lung homogenates. The antibodies were UCP2 mouse monoclonal antibody and voltage-dependent anion channel (VDAC) rabbit polyclonal antibody. Lanes were run on the same gel. Vertical line indicates the lanes are not contiguous. Results were identical for IB using UCP2 goat polyclonal antibody (data not shown). SI, siUCP2; SC, scRNA. *$P < 0.05$ versus scRNA. (**C**) Bars show effects of indicated treatments following alveolar HCl or microvascular H_2O_2 injections. KO, endothelial cell–specific *UCP2*-KO; LM, littermate control. For each pair, *$P < 0.05$ versus left bar. (**D**) Confocal images show dextran distribution at indicated locations. The endothelial cytosol was loaded with CR. FITC-D70 was infused in vessels at baseline and then again after injection of alveolar HCl. Scale bar: 20 μm. (**E**) Bars quantify FITC-D70–filled alveoli (edematous alveoli) following the indicated alveolar injections. Equal numbers of alveoli were injected in each group. Alveoli with greater than 50% luminal area filled with FITC-D70 were defined as edematous. UN, untreated. *$P < 0.05$ versus PBS. Data are shown as mean ± SEM for the number of injections indicated by dots. n, number of lungs. One-way ANOVA with post hoc Bonferroni's test was used to determine statistical differences between groups.

fluorescence leak (Figure 2, D and E). By contrast, alveolar HCl injection caused marked transvascular leakage and alveolar entry of FITC-D70, an effect that was sustained for a further 30 minutes (Figure 2E). Hence, different from rat lungs (1), alveolar HCl injection in mouse lungs rapidly induced endothelial barrier loss, leading to sustained alveolar edema, suggesting the difference was species dependent.

We considered that endothelial mitochondrial depolarization due to UCP2 activation could compromise mitochondrial calcium buffering (15), leading to loss of endothelial barrier properties. In lungs with UCP2-KD in the endothelium, alveolar microinjection of HCl did not cause microvascular leakage of FITC-D70 (Figure 2, D and E). The leakage was evident after scRNA treatment, ruling out nonspecific effects. These findings indicate that alveolar injection of HCl caused UCP2-dependent microvascular hyperpermeability.

To determine the UCP2 role in acid-induced ALI, we gave mice intranasal HCl (16). Then 2 hours later, we quantified cell counts and protein content in the bronchoalveolar lavage (BAL) and extravascular lung water (EVLW) in lung homogenates (1). In untreated mice, or in mice treated with scrambled siRNA, HCl increased cell counts and protein content in the BAL (Figure 3, A and B), indicating presence of lung inflammation and alveolar protein permeability. Moreover, EVLW increased (Figure 3C), consistent with the notion that HCl causes lung injury. By contrast, following UCP2 knockdown by siUCP2 treatment, all HCl-induced effects were markedly inhibited. Thus, BAL protein content was not different from controls, and the increase in BAL cell counts, though statistically significant ($P < 0.05$), was considerably lower than that of untreated controls. Importantly, EVLW did not increase significantly. These findings mechanistically implicated UCP2 activation in the HCl-induced increases of BAL cell count, protein content, and EVLW. We conclude that alveolar HCl–induced UCP2 activation caused global loss of endothelial barrier function in the lung, resulting in pulmonary edema.

Actin depolymerization underlies alveolar acid–induced hyperpermeability. Because the HCl-induced endothelial barrier loss was rapid, we considered that alveolar HCl might induce an endothelial signaling pathway through actin depolymerization, thereby destabilizing the barrier (17). Endothelial actin depolymerization could occur by known alveolar HCl–induced endothelial Ca^{2+} increases (1), activating the Ca^{2+}-dependent phosphatase, calcineurin. Calcineurin dephosphorylates cofilin, causing actin depolymerization (18, 19). The alveolar HCl–induced FITC-D70 hyperpermeability was absent in microvessels pretreated with the calcineurin inhibitor, tacrolimus, implicating calcineurin in the barrier effect. Subsequently, we transfected the lung capillary endothelium to express constitutively inactive cofilin (inCFLN, Figure 4A), which cannot depolymerize actin (20). Alveolar HCl–induced FITC-D70 hyperpermeability was absent following inCFLN transfection (Figure 4B). To rule out nonspecific effects, we confirmed that transfection of WT cofilin had no effect on the HCl-induced hyperpermeability (data not shown). We then assessed the actin response in lung capillaries. Alveolar HCl injection decreased endothelial F-actin within 20 minutes, as indicated by loss of rhodamine phalloidin fluorescence (Figure 4, C and D). This effect was absent in inCFLN-expressing (Figure 4D), but not WT cofilin–expressing, microvessels (data not shown). Taken together, these findings support what we believe is a novel role for the calcineurin-cofilin-actin axis in alveolar HCl–induced endothelial barrier failure.

Discussion

Our findings reveal the understanding that acid-induced alveolar injury induces a remarkably rapid hyperpermeability response in lung microvessels. Acid contact with the alveolar epithelium caused the expected fast, but quickly repaired, apical injury, resulting in calcium-induced H_2O_2 release (1) (Figure 5A). H_2O_2 is thought to induce hyperpermeability through tyrosine phosphorylation of barrier regulatory proteins (21). However, our surprising finding was that a major effect of the epithelium-derived H_2O_2 was to rapidly depolarize endothelial mitochondria (Figure 5B). Although the depolarization also recovered quickly, its duration was sufficient to induce cytoskeletal destabilization, causing endothelial barrier deterioration and alveolar edema (Figure 5C). Thus, the transient mitochondrial depolarization induced an H_2O_2-activated barrier switch that increased transvascular fluid flux.

To our knowledge, these are the first findings to mechanistically link endothelial UCP2 to microvascular hyperpermeability. Although UCP2 expression is reported in lung (22–25), endothelium (26, 27), and immune cells (28), its mechanistic role in lung injury is unclear because UCP2 expression may protect against (29), or exacerbate (30, 31), the injury. It is understood that UCP2 activation in the IMM occurs as negative feedback to protect mitochondria from the damaging effects of increased mitochondrial ROS production in the electron transport chain (7). UCP2 activation dissipates the proton gradient across the IMM, decreasing ROS production. However, the unexpected finding here was that although the H_2O_2 was extra-endothelial, hence not of endothelial mitochondrial origin, UCP2 activation occurred nevertheless.

We affirmed the UCP2 role through knockdown and endothelium-specific KO studies, providing definitive evidence that UCP2 was the key player in the mitochondrial depolarization. Inhibition of UCP2 activation prevented acid-induced microvascular hyperpermeability, as indicated by dextran extravasation and lung water quantification, further underlining UCP2's role in the barrier effect. Peroxisomal catalase is expected to protect mitochondria from the damaging effects of extramitochondrial H_2O_2 through catalase-induced hydrolysis. This protection may not be entirely applicable to microvessels because in at least 2 instances, namely epithelium-derived H_2O_2 induced by alveolar acid and direct microvascular H_2O_2 infusion, sufficient H_2O_2 reached endothelial mitochondria to cause UCP2 activation. These findings suggest that endothelial mitochondria of lung capillaries are susceptible to the effects of extra-endothelial H_2O_2 that might be produced under inflammatory conditions. The basis of this susceptibility requires further study.

A novel (to our knowledge) understanding that emerges from our findings relates to loss of the mitochondrial calcium buffering capacity as a barrier regulatory mechanism. The buffering capacity is a major mitochondrial function by which mitochondria take up calcium through the mitochondrial calcium uniporter, preventing potentially cell-injurious increases in the cytosolic calcium (15, 32). Mitochondrial depolarization blocks the mitochondrial buffering capacity (15). Hence, cytosolic calcium increases, resulting in the activation of calcium-dependent responses, including the activation of the phosphatase calcineurin (33). An important consequence of this activation is the dephosphorylation of cofilin, a calcineurin target. Cofilin dephosphorylation causes actin depolymerization (18, 19), potentially weakening barrier-stabilizing protein-protein interactions.

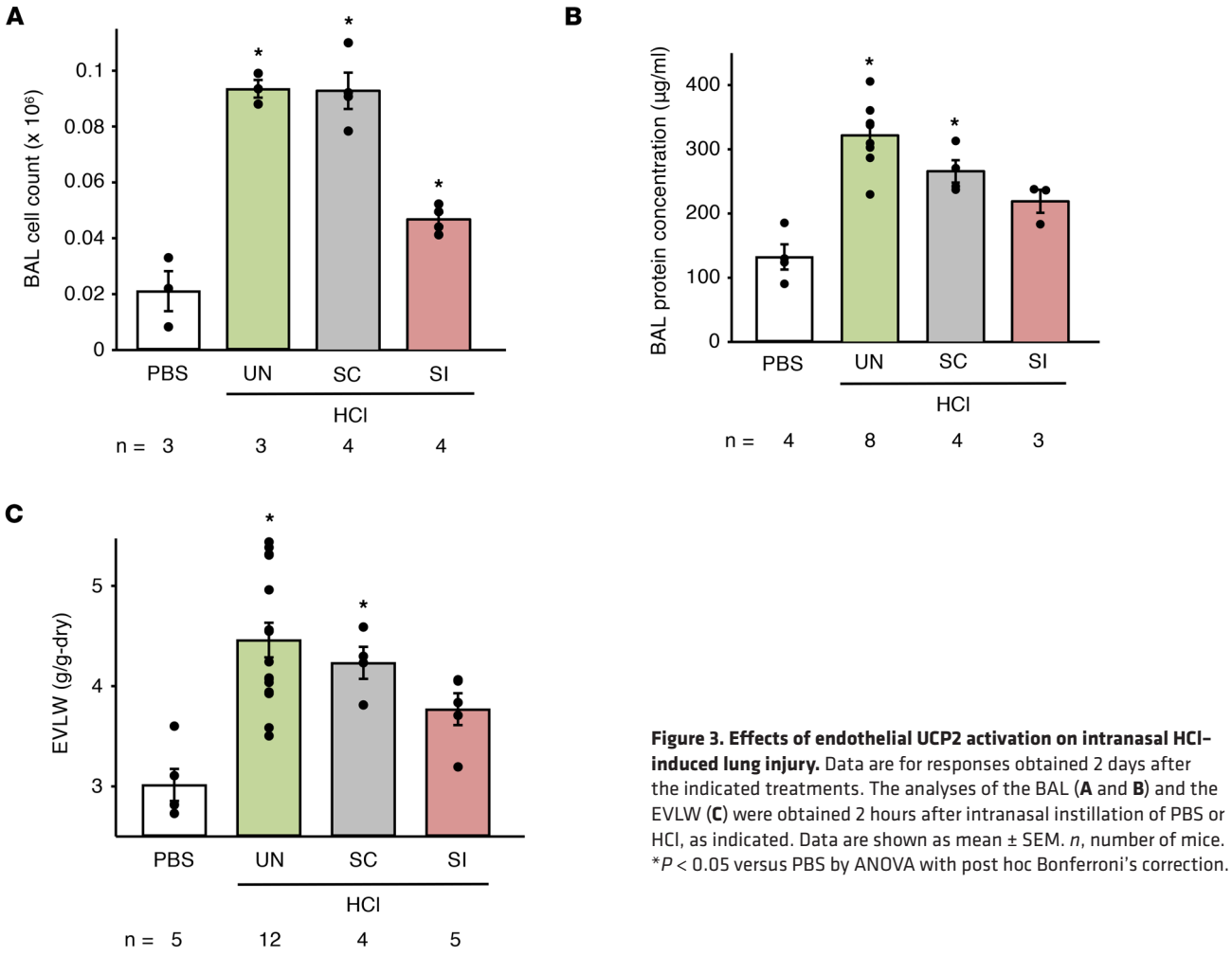

Figure 3. Effects of endothelial UCP2 activation on intranasal HCl–induced lung injury. Data are for responses obtained 2 days after the indicated treatments. The analyses of the BAL (**A** and **B**) and the EVLW (**C**) were obtained 2 hours after intranasal instillation of PBS or HCl, as indicated. Data are shown as mean ± SEM. *n*, number of mice. *$P < 0.05$ versus PBS by ANOVA with post hoc Bonferroni's correction.

Our findings support the calcineurin-cofilin-actin mechanism of barrier regulation. Actin polymerization can cause stress fiber formation, inducing barrier deterioration through the actomyosin mechanism (34, 35). However, a different mechanism might also apply, involving the subcortical F-actin layer that stabilizes the barrier (17). Enhancing this F-actin layer enhances the density of barrier proteins, strengthening the barrier (17). Our findings indicate that the opposite is also true, namely that decreasing the F-actin layer weakens the barrier. Thus, we show here that actin depolymerization caused by cofilin dephosphorylation led to loss of endothelial barrier properties and that the calcineurin inhibitor, tacrolimus, inhibited acid-induced edema. Thus, although both anti- (36) and pro-endothelial barrier (37–39) effects of calcineurin are reported, our studies support an anti-barrier role. Hence, we propose that the present UCP2-induced barrier loss occurred as a consequence not of the traditionally understood stress fiber–actomyosin mechanism, but of a calcineurin-cofilin mechanism that destabilized the cortical F-actin layer. However, further studies are required to better understand calcineurin-dependent barrier regulation.

Our findings contribute to the overall understanding of acid-induced ALI. In agreement with 6-hour determinations after acid instillation by Folkesson et al. (3), we find that the lung water increase at 2 hours was mild and unlikely to be lethal. By contrast, Zarbock et al. reported mortality in mice 3 hours after acid instillation (40). However, these authors also injected a large volume of intratracheal air that could have contributed to the injury. We note that UCP2 knockdown diminished leukocyte infiltration into the lung 2 hours after acid instillation, suggesting that endothelial mitochondrial depolarization promotes expression of leukocyte adhesion receptors. Underlying mechanisms for this effect require further understanding.

Although our interpretations are endothelium specific, nonendothelial mechanisms of acid-induced ALI require consideration, including the roles of neutrophils (3, 40), epithelial edema clearance (41), and

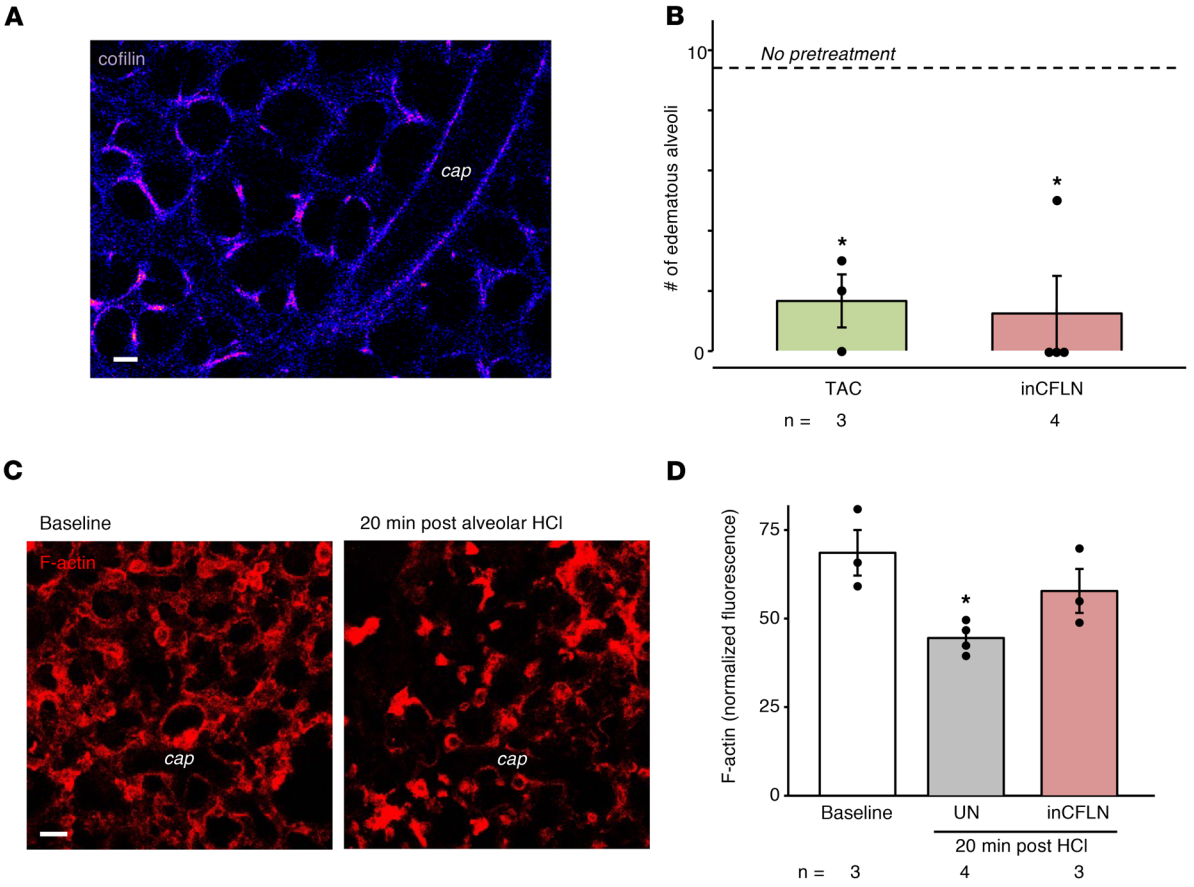

Figure 4. Alveolar HCl–induced activation of the calcineurin-cofilin-actin pathway in the endothelium. (**A**) Confocal image shows endothelial fluorescence of cofilin-GFP. *n* = 5. Scale bar: 20 μm. (**B**) Bars are counts of edematous alveoli (>50% FITC-D70 filling) following alveolar HCl after indicated pretreatments. inCFLN, inactive cofilin; TAC, tacrolimus (60 μM, 30 minutes). **P* < 0.05 versus HCl alone (dashed line). (**C**) Images show endothelial F-actin distribution before and after alveolar HCl injection. Lung capillaries were microinfused with 4% paraformaldehyde and 0.2% Triton X-100 (20 minutes), then with rhodamine phalloidin (1 U/ml, 5 minutes). Scale bar: 20 μm. (**D**) Bars quantify F-actin responses in terms of rhodamine phalloidin fluorescence normalized to nuclear fluorescence of Hoechst 33342 (not shown). **P* < 0.05 versus baseline. Data are shown as mean ± SEM for the number of injections indicated by dots. *n*, number of lungs. One-way ANOVA with post hoc Bonferroni's correction was used to determine statistical differences between groups.

apoptosis (42). Regarding neutrophils, neutrophil-induced microvascular injury occurs with delays longer than the present time course (3, 43). Moreover, neutrophils were not evident in the optically viewed microvessels that nevertheless underwent barrier loss. We note that in studies in which IPLs were continuously weighed, acid instillation caused weight increases within minutes (2). This rapid weight increase also suggests that acid-induced pulmonary edema occurred rapidly, well before neutrophils could be recruited. It is possible that at later time points, neutrophils may become a source for mitochondria-depolarizing H_2O_2. Regarding edema clearance, this mechanism is implicated in lung injury at about 6 hours after alveolar acid instillation (41). However, here, endothelium-specific UCP2 knockdown, or KO, blocked alveolar edema occurring within 30 minutes, indicating that the edema was a specific endothelium-dependent effect, ruling out epithelial mechanisms. Regarding apoptosis, because our studies show recovery of mitochondrial polarity, we conclude there was no apoptosis in that mitochondrial potential does not recover (44). Further, mitochondria-dependent apoptosis takes hours to develop (11, 45); hence, this mechanism is probably not relevant to short-term responses we report here. However, it is possible that at time points later than those of our study, nonendothelial mechanisms may assume a more prominent role in the injury.

Our ability to detect early mechanisms of barrier failure was attributable to our application of the live-lung optical imaging approach in conjunction with the lung micropuncture technique. Optical imaging allowed direct visualization of the epithelial-endothelial junction in the alveolar wall. Micropuncture enabled direct delivery of acid to the alveolar compartment. Further, micropuncture enabled the delivery of differently colored dyes to the alveolar and vascular compartments to load the epithelium and the endothelium, respectively.

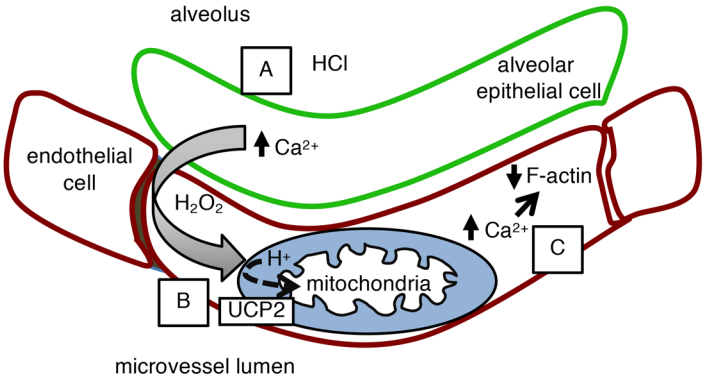

Figure 5. Proposed sequence of events in early alveolar HCl–induced endothelial hyperpermeability. (**A**) HCl contact with the alveolar epithelium causes pore formation and NOX2-induced diffusion of H_2O_2 to the capillary endothelium (1). (**B**) H_2O_2 activates endothelial UCP2, causing mitochondrial proton entry and depolarization. (**C**) Loss of mitochondrial potential leads to increases in cytosolic Ca^{2+}, which depolymerizes F-actin by a calcineurin-cofilin mechanism. F-actin decrease causes endothelial hyperpermeability.

It is well understood that the alveolar epithelium is highly impermeable to aqueous solutions. In confirmation, the absence of dye overlap indicated the absence of intercompartmental dye leakage. Importantly, acid injections in the alveolar compartment were restricted compartmentally because cellular injury occurred to the alveolar epithelium, but not to the adjoining endothelium. These findings raise the possibility of a disease model in which airway pathogens cause a compartmentally restricted injury to the alveolar epithelium, while the uninjured endothelium responds through cross-compartmental signaling.

Our study has potential limitations. Many findings were obtained by alveolar micropuncture of acid, a procedure that may damage the alveolar epithelium. However, cell membranes, including the alveolar epithelium, are known to self-repair rapidly (1, 46). Thus, we show that the endothelium and the epithelium of the alveolar wall can be discreetly loaded with cytosolic dyes that do not overlap fluorescence. Moreover, there was no time-dependent loss of cytosolic dye. Together these considerations rule out the possibility that alveolar micropuncture caused cellular damage. Our studies were restricted to a 2-hour period of observations. Further studies are therefore required to address the UCP2 hypothesis for longer periods into the induced injury, in acid aspiration and other models of ALI.

Because the alveolar epithelium contains mitochondria, a potential role for the epithelial UCP2 in the present responses requires consideration. Since we gave liposome-conjugated siRNA by the intravascular route, the question arises as to whether the liposomes crossed the endothelial barrier to reach the alveolar epithelium, thereby knocking down epithelial UCP2. However, such a liposome transit is unlikely because the endothelial barrier poses steric hindrance. The liposomes, which tend to be greater than 100 nm in diameter, are too large to cross the endothelial barrier that permits transit only of molecules of diameter less than 5 nm. Therefore, it is highly unlikely that the intravascular liposomes reached the alveolar epithelium. Consistent with this premise, intravascular siRNA delivery failed to block the HCl-induced mitochondrial depolarization in the alveolar epithelium. Taking these considerations together, we interpret that the UCP2 knockdown was restricted to the endothelium and that off-target effects in the alveolar epithelium were absent. However, these issues require further study.

In conclusion, our findings extend the understanding of the mitochondrial role in endothelial barrier regulation. Previously, mitochondria have been implicated in alveolar repair because transfer of functional mitochondria to the epithelium protected against ALI-induced mortality (9). Our present findings implicating UCP2-induced mitochondrial depolarization in endothelial barrier failure indicate that better understanding is required as to how UCP2 affects longer term outcomes in ALI. For example, persistent alveolar injury may maintain UCP2 activation, sustaining the microvascular hyperpermeability that causes life-threatening outcomes in ALI. Thus, further understanding is required as to whether UCP2 inhibition constitutes a potential therapeutic strategy for ALI.

Methods

Fluorophores. TMRE, calcein AM, calcein red-orange AM, CellTracker Deep Red, and rhodamine phalloidin were purchased from Thermo Fisher Scientific. FITC-conjugated dextran was purchased from Sigma-Aldrich.

Antibodies, siRNA, and plasmids. UCP2 goat polyclonal antibody (catalog sc-6525), UCP2 mouse monoclonal antibody (catalog sc-390189), and VDAC mouse monoclonal antibody (catalog sc-390996)

were purchased from Santa Cruz Biotechnology. VDAC rabbit polyclonal antibody (catalog 4866) was purchased from Cell Signaling Technology. IRDye 680LT goat anti-rabbit (catalog 925-68021), IRDye 800CW goat anti-mouse (catalog 926-32210), and IRDye 800CW donkey anti-goat (catalog 926-32214) were purchased from LI-COR. UCP2 siRNA (catalog AM16708, siRNA ID 187489) and scRNA were purchased from Thermo Fisher Scientific. scRNA was designed using GenScript's siRNA Sequence Scramble with the sequence (5′>3′) ACUACGGCCGAACCAUACUtt (sense) and (5′>3′) AGUAUGGUUCGGCCGUAGUtt (antisense). Catalase construct (47) was provided by J.A. Melendez (Albany Medical College, Albany, New York, USA) and subcloned as previously described (13) into the pBI-CMV bidirectional vector expressing the fluorescent protein DsRed. WT cofilin and inCFLN S3E plasmids (20) were gifts of S.S. Martin (University of Maryland School of Medicine, Baltimore, Maryland, USA).

Agents. 10N HCl and BAPTA-AM were purchased from Thermo Fisher Scientific. Dulbecco's PBS was purchased from Corning. H_2O_2, tacrolimus, and NAC were purchased from Sigma-Aldrich.

Animals. Male Swiss Webster mice were purchased from Taconic Biosciences, and experiments were performed on mice aged 6–8 weeks (approximately 25–30 g). To obtain *UCP2$^{fl/fl}$:Tie2-Cre* mice, we bred UCP2-floxed mice (B6;129S mixed background, The Jackson Laboratory, catalog 022394) (48) with Tie2-Cre mice (49) obtained from C.P. Blobel (Hospital for Special Surgery, New York, New York, USA). Both sexes of transgenic mice were used at age 4 months (approximately 30 g).

Lung preparation. IPLs were prepared according to our previously reported methods (13). In brief, mice were anesthetized with ketamine and xylazine, and lungs were excised en bloc. Lungs were continuously perfused by peristaltic roller pump with autologous blood (hematocrit 10%) diluted in HEPES buffer, pH 7.4, containing 1% FBS and 4% 70-kDa dextran at a rate of 0.5 ml/min at 37°C. Lungs were constantly inflated through an airway cannula at a pressure of 5 cmH_2O; pulmonary artery and left atrial pressures were held at 10 and 3 cmH_2O, respectively.

Imaging. In situ fluorescence imaging was carried out using our previously described methods (13). Briefly, vessels were loaded by 20-minute infusions of fluorophores, followed by 10-minute buffer wash, except where stated. Alveoli were loaded by 10-minute infusions of fluorophores, except where stated. Alveoli and microvessels were viewed by confocal microscopy (Zeiss LSM 510 and Leica SP8). In all experiments in which more than 1 dye was loaded, we confirmed the absence of bleed-through between fluorescence emission channels. Fluorescence was quantified using ImageJ software through analyses based on region of interest and line scan tools.

Labeling of UCP2 antibody. Alexa Fluor 633 carboxylic acid, succinimidyl ester, probe was used to label UCP2 primary antibody for immunofluorescence studies. Antibody was concentrated to 1.5–2.0 mg/ml, and buffer was exchanged with Ca^{2+}- and Mg^{2+}-free PBS using Vivaspin 500 concentrators (Lab Technology Products) at 4°C. To raise the pH to 9, 10 μl of 1 M $NaHCO_3$ was added to the antibody solution. Alexa Fluor dissolved in 10 μl (10 mg/ml) of anhydrous dimethylformamide was added to the reaction mixture. The reaction mixture was protected from light and mixed by vortex every 10 minutes at room temperature for 90 minutes. At the end of the reaction, unbound dye was separated using a Sephadex G-50 3-ml spin column (GE Healthcare Bio-Sciences AB) in PBS at 500 *g* for 5 minutes.

In vivo transfection. Stock solutions (1 μg/μl) of plasmids or siRNA were complexed with freshly extruded unilamellar liposomes (20 μg/μl, 100-nm pore size; DOTAP, Avanti Lipids) in sterile Opti-MEM (Life Technologies) to a final nucleic acid concentration of 0.3 μg/μl. Mice were given the nucleic acid/liposome mixture as an injection by tail vein for endothelial transfection or as an intranasal instillation for epithelial transfection. Lungs from transfected animals were excised 48 hours later.

Immunoblots. Lungs were homogenized (2-ml Dounce Glass Tissue Grinder), and mitochondria were isolated (Mitochondrial Isolation Kit for Tissue; Thermo Fisher Scientific). Equal amounts of protein from lysates were separated by SDS-PAGE, transferred onto nitrocellulose membrane at 4°C, and blocked in StartingBlock Blocking Buffer (Pierce), and then immunoblotting was performed.

Acid-instilled lung injury. As previously described (16), we held anesthetized mice (Swiss Webster; body weight 25–35 g) in a supine and inclined position on a thermal blanket (Harvard Apparatus Inc) set at 37°C. We intranasally instilled a bolus of 0.1N HCl, pH 1.1, in PBS at 2 ml/kg. Two hours later, EVLW measurements (1), and BAL cell count and protein content determinations (50), were performed as previously described.

Statistics. Data are shown as mean ± SEM of responses to the overall number of injections in each group of lungs. Each group consisted of at least 3 lungs. The numbers of lungs are indicated. Paired differences were compared by 2-tailed *t* test; group differences were analyzed by ANOVA with post hoc Bonferroni's correction. Significance was accepted at $P < 0.05$.

Study approval. All animal procedures were reviewed and approved by the Institutional Animal Care and Use Committee at Columbia University Medical Center.

Author contributions

RFH designed and carried out experiments, analyzed data, and wrote the manuscript. MNI and GAG contributed to the experimental design. GJ and SD provided reagents. JB supervised the overall project, designed experiments, and wrote the manuscript. All authors edited the manuscript.

Acknowledgments

The authors acknowledge M. Wei for assistance with genotyping. This work was supported by a Stony Wold - Herbert Fund, Inc. fellowship and NIH T32 Research Training Fellowship HL105323 to RFH, American Heart Association Grant-in-Aid 25740080 to MNI, and grants HL36024, HL57556, and HL122730 from the NIH to JB.

Address correspondence to: Jahar Bhattacharya, Department of Medicine, 630 W. 168th St., Room BB 8-812, New York, New York 10032, USA. Phone: 212.305.7093; Email: jb39@cumc.columbia.edu.

1. Westphalen K, Monma E, Islam MN, Bhattacharya J. Acid contact in the rodent pulmonary alveolus causes proinflammatory signaling by membrane pore formation. *Am J Physiol Lung Cell Mol Physiol*. 2012;303(2):L107–L116.
2. Nanjo S, Bhattacharya J, Staub NC. Concentrated albumin does not affect lung edema formation after acid instillation in the dog. *Am Rev Respir Dis*. 1983;128(5):884–889.
3. Folkesson HG, Matthay MA, Hébert CA, Broaddus VC. Acid aspiration-induced lung injury in rabbits is mediated by interleukin-8-dependent mechanisms. *J Clin Invest*. 1995;96(1):107–116.
4. Kuebler WM, Parthasarathi K, Wang PM, Bhattacharya J. A novel signaling mechanism between gas and blood compartments of the lung. *J Clin Invest*. 2000;105(7):905–913.
5. Schneeberger EE. Segmental differentiation of endothelial intercellular junctions in intra-acinar arteries and veins of the rat lung. *Circ Res*. 1981;49(5):1102–1111.
6. Echtay KS, et al. Superoxide activates mitochondrial uncoupling proteins. *Nature*. 2002;415(6867):96–99.
7. Mattiasson G, et al. Uncoupling protein-2 prevents neuronal death and diminishes brain dysfunction after stroke and brain trauma. *Nat Med*. 2003;9(8):1062–1068.
8. Mailloux RJ, Harper ME. Uncoupling proteins and the control of mitochondrial reactive oxygen species production. *Free Radic Biol Med*. 2011;51(6):1106–1115.
9. Islam MN, et al. Mitochondrial transfer from bone-marrow-derived stromal cells to pulmonary alveoli protects against acute lung injury. *Nat Med*. 2012;18(5):759–765.
10. Westphalen K, et al. Sessile alveolar macrophages communicate with alveolar epithelium to modulate immunity. *Nature*. 2014;506(7489):503–506.
11. Carroll RG, Hollville E, Martin SJ. Parkin sensitizes toward apoptosis induced by mitochondrial depolarization through promoting degradation of Mcl-1. *Cell Rep*. 2014;9(4):1538–1553.
12. Kisanuki YY, Hammer RE, Miyazaki J, Williams SC, Richardson JA, Yanagisawa M. Tie2-Cre transgenic mice: a new model for endothelial cell-lineage analysis in vivo. *Dev Biol*. 2001;230(2):230–242.
13. Rowlands DJ, et al. Activation of TNFR1 ectodomain shedding by mitochondrial Ca^{2+} determines the severity of inflammation in mouse lung microvessels. *J Clin Invest*. 2011;121(5):1986–1999.
14. Tang Y, Harrington A, Yang X, Friesel RE, Liaw L. The contribution of the Tie^{2+} lineage to primitive and definitive hematopoietic cells. *Genesis*. 2010;48(9):563–567.
15. Rizzuto R, De Stefani D, Raffaello A, Mammucari C. Mitochondria as sensors and regulators of calcium signalling. *Nat Rev Mol Cell Biol*. 2012;13(9):566–578.
16. Emin MT, Sun L, Huertas A, Das S, Bhattacharya J, Bhattacharya S. Platelets induce endothelial tissue factor expression in a mouse model of acid-induced lung injury. *Am J Physiol Lung Cell Mol Physiol*. 2012;302(11):L1209–L1220.
17. Quadri SK, Sun L, Islam MN, Shapiro L, Bhattacharya J. Cadherin selectivity filter regulates endothelial sieving properties. *Nat Commun*. 2012;3:1099.
18. Zhang XF, Hyland C, Van Goor D, Forscher P. Calcineurin-dependent cofilin activation and increased retrograde actin flow drive 5-HT-dependent neurite outgrowth in Aplysia bag cell neurons. *Mol Biol Cell*. 2012;23(24):4833–4848.
19. Descazeaud V, Mestre E, Marquet P, Essig M. Calcineurin regulation of cytoskeleton organization: a new paradigm to analyse the effects of calcineurin inhibitors on the kidney. *J Cell Mol Med*. 2012;16(2):218–227.
20. Vitolo MI, et al. Loss of PTEN induces microtentacles through PI3K-independent activation of cofilin. *Oncogene*. 2013;32(17):2200–2210.
21. Rhee SG, Bae YS, Lee SR, Kwon J. Hydrogen peroxide: a key messenger that modulates protein phosphorylation through cysteine oxidation. *Sci STKE*. 2000;2000(53):pe1.
22. Hidaka S, Kakuma T, Yoshimatsu H, Yasunaga S, Kurokawa M, Sakata T. Molecular cloning of rat uncoupling protein 2 cDNA and its expression in genetically obese Zucker fatty (fa/fa) rats. *Biochim Biophys Acta*. 1998;1389(3):178–186.
23. Hosoda K, et al. New members of uncoupling protein family implicated in energy metabolism. *Clin Exp Pharmacol Physiol*. 1999;26(7):561–562.

24. Pecqueur C, et al. Uncoupling protein 2, in vivo distribution, induction upon oxidative stress, and evidence for translational regulation. *J Biol Chem*. 2001;276(12):8705–8712.
25. Alán L, Smolková K, Kronusová E, Santorová J, Jezek P. Absolute levels of transcripts for mitochondrial uncoupling proteins UCP2, UCP3, UCP4, and UCP5 show different patterns in rat and mice tissues. *J Bioenerg Biomembr*. 2009;41(1):71–78.
26. Haslip M, et al. Endothelial uncoupling protein 2 regulates mitophagy and pulmonary hypertension during intermittent hypoxia. *Arterioscler Thromb Vasc Biol*. 2015;35(5):1166–1178.
27. Tian XY, et al. Uncoupling protein-2 protects endothelial function in diet-induced obese mice. *Circ Res*. 2012;110(9):1211–1216.
28. Fleury C, et al. Uncoupling protein-2: a novel gene linked to obesity and hyperinsulinemia. *Nat Genet*. 1997;15(3):269–272.
29. Tang SE, et al. Stanniocalcin-1 ameliorates lipopolysaccharide-induced pulmonary oxidative stress, inflammation, and apoptosis in mice. *Free Radic Biol Med*. 2014;71:321–331.
30. Wang Q, et al. Uncoupling protein 2 increases susceptibility to lipopolysaccharide-induced acute lung injury in mice. *Mediators Inflamm*. 2016;2016:9154230.
31. Yu SX, et al. Genipin inhibits NLRP3 and NLRC4 inflammasome activation via autophagy suppression. *Sci Rep*. 2015;5:17935.
32. Raffaello A, De Stefani D, Rizzuto R. The mitochondrial Ca(2+) uniporter. *Cell Calcium*. 2012;52(1):16–21.
33. Rusnak F, Mertz P. Calcineurin: form and function. *Physiol Rev*. 2000;80(4):1483–1521.
34. Goeckeler ZM, Wysolmerski RB. Myosin light chain kinase-regulated endothelial cell contraction: the relationship between isometric tension, actin polymerization, and myosin phosphorylation. *J Cell Biol*. 1995;130(3):613–627.
35. Mehta D, Malik AB. Signaling mechanisms regulating endothelial permeability. *Physiol Rev*. 2006;86(1):279–367.
36. Karpurapu M, et al. Inhibition of nuclear factor of activated T cells (NFAT) c3 activation attenuates acute lung injury and pulmonary edema in murine models of sepsis. *Oncotarget*. 2018;9(12):10606–10620.
37. Ikezoe T, Yang J, Nishioka C, Umezawa K, Yokoyama A. Thrombomodulin blocks calcineurin inhibitor-induced vascular permeability via inhibition of Src/VE-cadherin axis. *Bone Marrow Transplant*. 2017;52(2):245–251.
38. Kolozsvári B, et al. Calcineurin regulates endothelial barrier function by interaction with and dephosphorylation of myosin phosphatase. *Cardiovasc Res*. 2012;96(3):494–503.
39. Kolozsvári B, et al. Role of calcineurin in thrombin-mediated endothelial cell contraction. *Cytometry A*. 2009;75(5):405–411.
40. Zarbock A, Singbartl K, Ley K. Complete reversal of acid-induced acute lung injury by blocking of platelet-neutrophil aggregation. *J Clin Invest*. 2006;116(12):3211–3219.
41. Modelska K, Pittet JF, Folkesson HG, Courtney Broaddus V, Matthay MA. Acid-induced lung injury. Protective effect of anti-interleukin-8 pretreatment on alveolar epithelial barrier function in rabbits. *Am J Respir Crit Care Med*. 1999;160(5 pt 1):1450–1456.
42. Albertine KH, et al. Fas and fas ligand are up-regulated in pulmonary edema fluid and lung tissue of patients with acute lung injury and the acute respiratory distress syndrome. *Am J Pathol*. 2002;161(5):1783–1796.
43. Reutershan J, Basit A, Galkina EV, Ley K. Sequential recruitment of neutrophils into lung and bronchoalveolar lavage fluid in LPS-induced acute lung injury. *Am J Physiol Lung Cell Mol Physiol*. 2005;289(5):L807–L815.
44. Zamzami N, et al. Reduction in mitochondrial potential constitutes an early irreversible step of programmed lymphocyte death in vivo. *J Exp Med*. 1995;181(5):1661–1672.
45. Lin Z, et al. Suppression of GLI sensitizes medulloblastoma cells to mitochondria-mediated apoptosis. *J Cancer Res Clin Oncol*. 2016;142(12):2469–2478.
46. McNeil PL, Steinhardt RA. Plasma membrane disruption: repair, prevention, adaptation. *Annu Rev Cell Dev Biol*. 2003;19:697–731.
47. Bai J, Rodriguez AM, Melendez JA, Cederbaum AI. Overexpression of catalase in cytosolic or mitochondrial compartment protects HepG2 cells against oxidative injury. *J Biol Chem*. 1999;274(37):26217–26224.
48. Kong D, et al. Glucose stimulation of hypothalamic MCH neurons involves K(ATP) channels, is modulated by UCP2, and regulates peripheral glucose homeostasis. *Cell Metab*. 2010;12(5):545–552.
49. Weskamp G, et al. Pathological neovascularization is reduced by inactivation of ADAM17 in endothelial cells but not in pericytes. *Circ Res*. 2010;106(5):932–940.
50. Hook JL, Islam MN, Parker D, Prince AS, Bhattacharya S, Bhattacharya J. Disruption of staphylococcal aggregation protects against lethal lung injury. *J Clin Invest*. 2018;128(3):1074–1086.